



Informative path planning for anomaly detection in environment exploration and monitoring

Antoine Blanchard^{*}, Themistoklis Sapsis

Department of Mechanical Engineering, Massachusetts Institute of Technology, Cambridge, MA 02139, United States of America

ARTICLE INFO

Keywords:

Informative path planning
Extreme anomaly detection
Bayesian optimization
Environment exploration
Adversarial conditions

ABSTRACT

An unmanned autonomous vehicle (UAV) is sent on a mission to explore and reconstruct an unknown environment from a series of measurements collected by Bayesian optimization. The success of the mission is judged by the UAV's ability to faithfully reconstruct any anomalous features present in the environment, with emphasis on the extremes (e.g., extreme topographic depressions or abnormal chemical concentrations). We show that the criteria commonly used for determining which locations the UAV should visit are ill-suited for this task. We introduce a number of novel criteria that guide the UAV toward regions of strong anomalies by leveraging previously collected information in a mathematically elegant and computationally tractable manner. We demonstrate superiority of the proposed approach in several applications, including reconstruction of seafloor topography from real-world bathymetry data, as well as tracking of dynamic anomalies. A particularly attractive property of our approach is its ability to overcome adversarial conditions, that is, situations in which prior beliefs about the locations of the extremes are imprecise or erroneous.

1. Introduction

With the rise of automation and artificial intelligence, a growing number of tasks deemed too tedious or too perilous for humans have been delegated to unmanned autonomous vehicles (UAV). This includes missions related to environment exploration and monitoring in which a UAV is tasked with producing a map for a quantity of interest (e.g., pollutant concentration, terrain elevation, or vegetation growth) by collecting measurements at various locations across a region of interest (e.g., a reservoir, a city, or a crop) (Singh et al., 2010; Dunbabin and Marques, 2012; Marchant and Ramos, 2012; Hitz et al., 2017; Flaspohler et al., 2018). The data collected by the UAV can be used to construct a statistical model for the quantity of interest, which in turn can be used for analysis and policy making. Of course, the statistical model is only as good as the measurements made by the UAV. Therefore, the question of data collection (i.e., how, when, and where to make measurements) is of paramount importance, especially from the standpoint of detecting *anomalies* in the environment.

Path-planning algorithms for environment exploration come in two flavors. Approaches in which the UAV decides on its next move one step at a time are referred to as *myopic* (Stachniss et al., 2005; Marchant and Ramos, 2014). Myopic algorithms are suitable for most situations but lack a mechanism for anticipation, which may be problematic in cases where path-planning decisions may have negative long-term consequences (e.g., the UAV gets stuck because of maneuverability

constraints). On the other hand, *non-myopic* algorithms operate on sequences of destinations, which allows them to look further into the future (Meliou et al., 2007; Singh et al., 2009; Morere et al., 2016, 2017). The main tool for this is the *partially observable Markov decision process*, which assigns a reward to each admissible sequence of actions. Non-myopic approaches are computationally complex and incredibly expensive, which is why myopic approaches are often preferred—including in the present work. We note, however, that the ideas presented here can be extended to the non-myopic setting (e.g., by adapting the BO-POMDP algorithm of Morere et al., 2017) notwithstanding the higher computational complexity.

The flagship feature of myopic algorithms is that they naturally lend themselves to Bayesian optimization (Brochu et al., 2010; Shahriari et al., 2015), allowing the UAV to (a) incorporate prior belief about the environment, and (b) decide on its next move by compromising between exploration of the space and exploitation of the available information. At the heart of Bayesian optimization is the acquisition function, which guides the UAV throughout the mission. Many acquisition functions have been proposed for environment exploration (Martinez-Cantin et al., 2009; Marchant and Ramos, 2012, 2014; Bai et al., 2016; Morere et al., 2017) but they all have one major flaw, namely, they have no robust mechanism to identify anomalous environmental features. For example, the approach of Marchant and

^{*} Corresponding author.

E-mail address: ablancha@mit.edu (A. Blanchard).

Ramos (2012) requires the user to specify the values of two ad hoc parameters which must be tuned on a case-by-case basis, with no foolproof guidelines on how to do so.

The main contribution of this work is the introduction of two novel acquisition functions that are specifically designed for anomaly detection in environment exploration. The proposed acquisition functions have the following advantages:

1. They are based on a probabilistic treatment of what constitutes an anomaly, thereby eliminating the need for ad hoc parameters;
2. Their computational complexity is comparable with that of traditional acquisition functions, making them suitable for online path planning and monitoring;
3. They provide the UAV operator with a mechanism to instill any prior beliefs they may have about the locations of anomalies while allowing the UAV to *correct and refine* the operator beliefs “on the fly” as more information is collected.

The remainder of the paper is structured as follows. We present the problem and approach in Section 2, introduce the acquisition functions in Section 3, evaluate their performance in Section 4, and offer some conclusions in Section 5.

2. Problem formulation and approach

2.1. Formulation of the problem

We consider the problem of environment exploration in which a UAV is tasked with reconstructing the spatiotemporal distribution of a quantity of interest $f : \mathbb{R}^2 \times \mathbb{R}^+ \rightarrow \mathbb{R}$ over a region of interest $\mathcal{Z} \subset \mathbb{R}^2$ and a time interval of interest $[0, T] \subset \mathbb{R}^+$. (We assume that f is Lipschitz continuous and \mathcal{Z} is compact.) To reconstruct the map f , the UAV is allowed to explore the space \mathcal{Z} and collect measurements at locations it deems informative. Uncertainty in observations is modeled with additive Gaussian noise, so that each measurement made by the UAV can be written as

$$y = f(\mathbf{z}, t) + \varepsilon, \quad \varepsilon \sim \mathcal{N}(0, \sigma_n^2), \quad (1)$$

where $\mathbf{z} = [z_1, z_2]^\top$ is a vector of coordinates identifying the UAV’s position in the Euclidean plane, and t is the time variable. The combination of position \mathbf{z} and orientation θ (with $\theta = 0$ taken to coincide with the z_1 -axis) completely determines the *pose* of the UAV. In what follows we will find it useful sometimes to view f as a function of a single input vector $\mathbf{x} = \{\mathbf{z}, t\}$.

The two key issues in environment reconstruction are data acquisition (i.e., when and where to collect measurements) and environment modeling (i.e., how to leverage measurements to construct an accurate model of the environment). From a modeling perspective, the challenge is to predict the value of a process that depends on space *and* time given a limited number of measurement points. Notable approaches for spatiotemporal modeling include space–time process convolutions (Higdon, 2002) and kernel extrapolation methods for distribution mapping algorithms (Reggente and Lilienthal, 2009), but the most popular of all is arguably Gaussian process (GP) regression, which we briefly review in Section 2.2. From a data-acquisition perspective, the challenge is to identify the locations that provide the most information about the underlying environmental process. This question, central to the present work, is discussed in Section 2.3 and the subsequent sections.

2.2. Gaussian process regression for environment modeling

To reconstruct the latent function f from a limited number of noisy measurements, a natural solution is to use a surrogate model, which we denote by \tilde{f} . In this work we use Gaussian process (GP) regression (Rasmussen and Williams, 2006), which has several advantages in the context of environment reconstruction. First, GPs are

agnostic to the internal intricacies of the unknown map f . Second, they allow for rigorous quantification of measurement uncertainty. Third, they are equipped with a mechanism that takes into account possible correlations across space and time, allowing them to deliver good performance on spatially-correlated data (Singh et al., 2010; Marchant and Ramos, 2014). Fourth, they are robust, versatile, easy to implement, and inexpensive to train when the input dimension and number of measurement points are not too large. For spatiotemporal processes the input dimension never exceeds four, i.e., at most three spatial dimensions and one temporal dimension.

For a dataset $\mathcal{D} = \{\mathbf{X}, \mathbf{y}\}$ of input–output pairs and a zero-mean GP with covariance function $k(\mathbf{x}, \mathbf{x}')$, the GP posterior mean and variance are given by

$$\mu(\mathbf{x}) = k(\mathbf{x}, \mathbf{X})\mathbf{K}^{-1}\mathbf{y}, \quad (2a)$$

$$\sigma^2(\mathbf{x}) = k(\mathbf{x}, \mathbf{x}) - k(\mathbf{x}, \mathbf{X})\mathbf{K}^{-1}k(\mathbf{X}, \mathbf{x}), \quad (2b)$$

respectively, where $\mathbf{K} = k(\mathbf{X}, \mathbf{X}) + \sigma_n^2\mathbf{I}$. As discussed in Section 2.1, here the input variable \mathbf{x} belongs to an augmented space which is constructed by appending the time variable t to the physical variables \mathbf{z} . Consequently, GP regression allows to infer the value of the latent function f at any spatial location, but also at any point in time, past or future.

In GP regression, the covariance function is the main building block for practitioners to encode structure (e.g., symmetry or invariance) in the model. For time-dependent environments, it is common to distinguish between separable and non-separable covariance functions (Marchant and Ramos, 2014). The former take the general form $k(\mathbf{x}, \mathbf{x}') = k(\mathbf{z}, \mathbf{z}')k(t, t')$ and are useful when the spatial variables are decoupled from the temporal variable in the latent function (Marchant and Ramos, 2014). In general, however, the coupling between space and time in the environment is complex or unknown, and as a result it is often preferable to use a non-separable covariance function. In this work we use a radial-basis-function (RBF) kernel with automatic relevance determination,

$$k(\mathbf{x}, \mathbf{x}') = \sigma_f^2 \exp[-(\mathbf{x} - \mathbf{x}')^\top \Theta^{-1}(\mathbf{x} - \mathbf{x}')/2], \quad (3)$$

where Θ is a diagonal matrix containing the lengthscales for each dimension and σ_f^2 is a scaling parameter. For a given dataset, the hyper-parameters $\{\sigma_f^2, \Theta\}$ are trained by maximum likelihood estimation (Rasmussen and Williams, 2006).

2.3. Bayesian optimization for informative path planning

The next question is to design an optimal strategy for data acquisition. As discussed in Section 2.1, the challenge is to select sensing locations in such a way that the resulting surrogate model is of sufficiently high fidelity across the region and time interval of interest. One simple strategy is for the UAV to visit a large number of precomputed locations that densely cover the search space, which is essentially equivalent to having a fixed network of sensors (Guestrin et al., 2005). In practice, however, this approach is intractable because exploration missions are always done on a budget with limited time and resources.

A better strategy is for the UAV to proceed sequentially and decide on its next destination based on the information it has collected so far. This information can be leveraged to improve the surrogate model \tilde{f} in real time. At each step, the next destination is selected by minimizing an acquisition function $a : \mathbb{R}^2 \times \mathbb{R}^+ \rightarrow \mathbb{R}$ which helps the UAV scout the environment. Once the allocated budget is exhausted, the mission is terminated and the surrogate model constructed by the UAV can be used in analyses as a substitute for the unknown map f (Algorithm 1). This algorithm is at the foundation of Bayesian optimization (Krause and Ong, 2011; Shahriari et al., 2015). Its success is conditioned on two key components: (a) the surrogate model \tilde{f} , which encapsulates the UAV’s belief about the structure of the environment given the data

Algorithm 1 Bayesian optimization for the “next-best-view” problem.

```

1: Input: Mission duration  $T$ , initial UAV position  $\mathbf{z}_0$  and orientation  $\theta_0$ , initial dataset  $\mathcal{D} = \{\mathbf{x}_i, y_i\}_{i=1}^{n_{init}}$ 
2: Initialize: Surrogate model  $\bar{f}$  trained on  $\mathcal{D}$ 
3: while  $t \leq T$  do
4:   Select next destination as  $\mathbf{z}_{n+1} = \arg \min_{\mathbf{z} \in \mathcal{Z}} a(\mathbf{z}, t; \bar{f}, \mathcal{D})$ 
5:   Record measurement  $y_{n+1}$  at  $\mathbf{x}_{n+1} = \{\mathbf{z}_{n+1}, t_{n+1}\}$ 
6:   Augment dataset:  $\mathcal{D} \leftarrow \mathcal{D} \cup \{\mathbf{x}_{n+1}, y_{n+1}\}$ 
7:   Update surrogate model
return Final surrogate model  $\bar{f}$ 

```

it has harnessed; and (b) the acquisition function a , upon which the UAV relies to plan its next move.

In practice the sampling frequency of the UAV sensors is much higher than the frequency of the decision making, and as a result the approach in Algorithm 1 is suboptimal because measurements are only collected at destination (Morere et al., 2017). Therefore, to replicate the conditions of an actual field experiment, we modify Algorithm 1 in two ways. First, we allow the UAV to collect measurements periodically (with sampling period t_s) as it travels from \mathbf{z}_n to \mathbf{z}_{n+1} . Second, to make the most of this additional data, we change the path-planning policy in Line 4 of Algorithm 1 to

$$\mathbf{z}_{n+1} = \arg \min_{\mathbf{z} \in \mathcal{Z}} \int_{S(\mathbf{z}_n, \mathbf{z})} a(\mathbf{z}, t; \bar{f}, \mathcal{D}_n) ds, \quad (4)$$

where $S(\mathbf{z}_n, \mathbf{z})$ denotes the path taken by the UAV to reach candidate destination \mathbf{z} from its current position \mathbf{z}_n . This approach, known as *informative path planning* (Morere et al., 2017), is summarized in Algorithm 2.

Algorithm 2 Bayesian optimization for informative path planning.

```

1: Input: Mission duration  $T$ , initial UAV position  $\mathbf{z}_0$  and orientation  $\theta_0$ , initial dataset  $\mathcal{D} = \{\mathbf{x}_i, y_i\}_{i=1}^{n_{init}}$ 
2: Initialize: Surrogate model  $\bar{f}$  trained on  $\mathcal{D}$ 
3: while  $t \leq T$  do
4:   Select next destination as in (4)
5:   while traveling from  $\mathbf{z}_n$  to  $\mathbf{z}_{n+1}$  do
6:     if  $\text{mod}(t, t_s) = 0$  then
7:       Record measurement  $y_i$  at  $\mathbf{x}_i = \{\mathbf{z}_i, t\}$ 
8:       Augment dataset:  $\mathcal{D} \leftarrow \mathcal{D} \cup \{\mathbf{x}_i, y_i\}$ 
9:   Update surrogate model
return Final surrogate model  $\bar{f}$ 

```

The primary difference between the traditional “next-best-view” problem (Algorithm 1) and the informative path-planning approach (Algorithm 2) is that the latter takes into account the UAV path in the calculation of the next destination. This allows the UAV to optimize its motion not only based on the expected value of the latent function at destination, but also based on the quality of the information the UAV is expecting to collect during its journey from \mathbf{z}_n to \mathbf{z}_{n+1} .

Typically the path $S(\mathbf{z}_n, \mathbf{z})$ is a parametric curve satisfying certain constraints related to continuity, smoothness, and curvature. For a given candidate destination \mathbf{z} , there is generally an infinite number of paths connecting \mathbf{z}_n and \mathbf{z} , so in practice the path parametrization is either specified in advance in a way that ensures uniqueness or optimized on the fly using an additional layer of optimization as in Marchant and Ramos (2014). (If one is willing to forego explicit parametrization of the path, then one may use a more sophisticated path-planning algorithm such as the HLT* algorithm (Zhang et al., 2019) or the visibility algorithm of Huang and Teo (2019) which are suitable for online rerouting.) In this work consecutive destinations are connected by a Dubins path with fixed turning radius along which the UAV travels at constant speed. Dubins paths are popular in robotics and

path planning owing to their simple geometric construction and computational tractability (Dubins, 1957). This parametrization ensures that the UAV path is C^1 -continuous.

As it stands, the path-planning policy (4) gives an unfair advantage to shorter routes over longer ones. A possible remedy is to normalize the integral in (4) by the path length. A more practice-driven approach is to restrict the set of admissible destinations to a subset $\mathcal{A}_n \subset \mathcal{Z}$, mimicking the fact that in practice the UAV has limited field of view and limited sensor range. This is the approach we will use in this work. We also note that for most acquisition functions, the integral in (4) is not analytic; in this work, we evaluate it using the trapezoidal rule.

2.4. Acquisition functions for environment exploration

We now address the question of data acquisition for environment reconstruction. The acquisition functions introduced below can be used “as is” in Algorithm 1, or as the integrand in (4) for use in Algorithm 2.

In environment exploration, the role of the acquisition function is to favor exploration of regions where uncertainty is high. We briefly review two common approaches to achieving this.

Uncertainty sampling (US). The most intuitive approach is for the UAV to go where the predictive variance of the GP model is the largest (MacKay, 1992), that is,

$$a_{US}(\mathbf{x}) = \sigma^2(\mathbf{x}). \quad (5)$$

This approach is tantamount to minimizing the mean squared error between \bar{f} and f (Kleijnen and Van Beers, 2004; Beck and Guillas, 2016), and therefore ensures that model uncertainty is distributed somewhat evenly over the search space.

Integrated variance reduction (IVR). Another approach is to consider the effect of observing a hypothetical “ghost” point \mathbf{x} on the overall model variance (Cohn, 1994). This effect is measured by

$$a_{IVR}(\mathbf{x}) = \int [\sigma^2(\mathbf{x}') - \sigma^2(\mathbf{x}'; \mathbf{x})] d\mathbf{x}' = \frac{1}{\sigma^2(\mathbf{x})} \int \text{cov}^2(\mathbf{x}, \mathbf{x}') d\mathbf{x}', \quad (6)$$

where $\sigma^2(\mathbf{x}'; \mathbf{x})$ is the predictive variance at \mathbf{x}' had \mathbf{x} been observed, and $\text{cov}^2(\mathbf{x}, \mathbf{x}')$ is the posterior covariance between \mathbf{x} and \mathbf{x}' (Gramacy and Lee, 2009; Blanchard and Sapsis, 2021b). Therefore, maximizing IVR has the effect of maximally reducing the overall model variance.

If the UAV operator wants to focus exploration on certain regions of the search space, or if they have prior beliefs about where relevant environmental features might be located, then it is possible to bias exploration by incorporating a prior $p_x(\mathbf{x})$ over the input space in US and IVR. The prior acts as a sampling weight, leading to

$$a_{US-IW}(\mathbf{x}) = \sigma^2(\mathbf{x}) p_x(\mathbf{x}), \quad (7)$$

$$a_{IVR-IW}(\mathbf{x}) = \frac{1}{\sigma^2(\mathbf{x})} \int \text{cov}^2(\mathbf{x}, \mathbf{x}') p_x(\mathbf{x}') d\mathbf{x}', \quad (8)$$

where the suffix “IW” stands for “input-weighted”. (That the prior appears as multiplicative factor for the (co)variance arises naturally from an expectation argument; more details can be found in Sacks et al. (1989) and Blanchard and Sapsis (2021b).) If \mathbf{x} carries contextual information in addition to spatial information, then the input prior can be decomposed as $p_x(\mathbf{x}) = p_z(\mathbf{z}) p_t(t)$, with the temporal prior p_t typically being uniform. If no prior knowledge is available, then p_z too can be chosen uniform, in which case US-IW and IVR-IW reduce to US and IVR, respectively.

The idea of using a prior as a sampling weight was first suggested by Sacks et al. (1989) in the context of sequential design of computer experiments. To the best of our knowledge, it has never been applied to problems related to environment exploration as a way of emphasizing certain regions of the input space. The closest instance of which we are aware is the work of Oliveira et al. (2019, 2020) in which a prior is used as a way to account for *localization noise*, that is, the error in

estimating the UAV position resulting from imperfections in the UAV sensors, actuators, and motion controllers. By contrast, in our approach we assume no localization noise and use the input prior as a mechanism to emphasize certain regions in the environment before the mission starts.

While other acquisition functions exist, either they are computationally more complex or they have narrower applicability than those previously discussed. For example, the mutual information, in general, cannot be written in closed form and thus loses out to US, the latter being a good approximation for the former (MacKay, 1992; Chaloner and Verdinelli, 1995). Likewise, the upper confidence bound (UCB), the expected improvement (EI), and the probability of improvement (PI) are not appropriate for environment reconstruction because they are designed for optimization, not exploration (Jones et al., 1998; Srinivas et al., 2009). And while UCB, EI and PI each contain an ad hoc parameter that governs the trade-off between exploration and exploitation, setting the value of that parameter to a large number in order to favor exploration is moot because in that limit UCB, EI and PI are equivalent to US (see Section S1 in the Supplementary Material). Variants of these criteria (Verdinelli and Kadane, 1992; Lam, 2008; Marchant and Ramos, 2012; Morere et al., 2017) suffer from the same shortcomings.

3. Methods

We are now in a position to introduce the acquisition functions that we will use for reconstruction of anomalous environment. Both share three critical features: (a) they leverage information collected previously by the UAV and skews exploration toward regions of the space where the map f is thought to exhibit strong anomalies; (b) they allow incorporation of a prior $p_x(\mathbf{x})$ over the search space, with expectations about potential benefits being similar to those discussed earlier for US-IW and IVR-IW; and (c) their computational complexity is comparable to that of traditional acquisition functions.

3.1. Output-informed acquisition functions for anomalous environment

We begin with a definition of what constitutes an anomalous environment. A map $f : \mathcal{X} \rightarrow \mathbb{R}$ is *anomalous* if the conditional probability density function (pdf) of the output $p_{f|\mathbf{x}}$ is heavy-tailed. Heavy tails are indicative of highly unlikely yet highly impactful events, and are therefore appropriate to characterize anomalies in output values. Heavy-tailed distributions are commonplace in applications related to risk (Embrechts et al., 2013) and extreme events (Albeverio et al., 2006) but as far as we know they have not been considered in the context of environment exploration. In what follows, we drop the conditional notation for clarity.

The proposed definition suggests a strategy for the UAV to decide on its next destination. At each iteration, the UAV can use the pdf of the GP mean p_μ as a proxy for p_f and select the next destination so that uncertainty in p_μ is most reduced. This strategy is similar to that of Mohamad and Sapsis (2018) but is not directly applicable to online path planning because of computability issues. However, as shown in Sapsis (2020) and Blanchard and Sapsis (2021a,b), it can be considerably simplified to produce the following acquisition function:

$$a_{IVR-LW}(\mathbf{x}) = \frac{1}{\sigma^2(\mathbf{x})} \int \text{cov}^2(\mathbf{x}, \mathbf{x}') \frac{p_x(\mathbf{x}')}{p_\mu(\mu(\mathbf{x}'))} d\mathbf{x}'. \quad (9)$$

Interestingly, Eq. (9) establishes a surprising connection between the approach in Mohamad and Sapsis (2018) and the IVR-based acquisition functions of Section 2.4. It should indeed be clear that (9) is related to (6) and (8), with the ratio $p_x(\mathbf{x})/p_\mu(\mu(\mathbf{x}))$ playing the role of a sampling weight.

In this work we also consider

$$a_{US-LW}(\mathbf{x}) = \sigma^2(\mathbf{x}) \frac{p_x(\mathbf{x})}{p_\mu(\mu(\mathbf{x}))} \quad (10)$$

as the “likelihood-weighted” (LW) counterpart of US and US-IW.

3.2. The likelihood ratio and its benefits

The quantity

$$w(\mathbf{x}) = \frac{p_x(\mathbf{x})}{p_\mu(\mu(\mathbf{x}))} \quad (11)$$

is commonly referred to as the *likelihood ratio* (Owen, 2013). When used in an acquisition function, it acts as a sampling weight, assigning to each point $\mathbf{x} \in \mathcal{X}$ a measure of *relevance* defined in probabilistic terms. Because of the presence of the output density p_μ in the denominator of (11), the likelihood ratio serves as an attention mechanism that promotes points associated with *abnormal* output values and penalizes points associated with frequent, average output values (Blanchard and Sapsis, 2021a,b).

In environment exploration, the likelihood ratio has numerous benefits. First, it incorporates field information through the GP mean $\mu(\mathbf{x})$ in such a way that (a) no additional ad hoc parameter is introduced; (b) anomalous regions are naturally accentuated due to the probabilistic dependence on the density p_μ ; and (c) it does not discriminate between abnormally small and abnormally large output values, which is a tremendous advantage over approaches based on PI, EI or UCB. Second, the likelihood ratio preserves the possibility for the operator to instill prior belief through the density p_x . But the fact that the input prior is weighted by the output density p_μ enables the UAV to *correct and refine* the operator’s beliefs on the fly as more information is collected. Thus, the likelihood ratio provides a mechanism for the UAV to strike an informed balance between its own representation of the environment and the operator’s guidelines. We will see that this feature significantly improves performance in *adversarial* situations, that is, situations where the operator’s beliefs are imprecise or erroneous.

We should not lose sight of the fact that these benefits may be neutralized if the likelihood ratio is not tractable computationally. Fortunately, that is not the case (Blanchard and Sapsis, 2021a,b). To evaluate (9) without resorting to Monte Carlo integration, we approximate the likelihood ratio with a Gaussian mixture model (GMM):

$$w(\mathbf{x}) \approx \sum_{i=1}^{n_{GMM}} \alpha_i \mathcal{N}(\mathbf{x}; \omega_i, \Sigma_i). \quad (12)$$

When combined with the RBF kernel, the GMM approximation renders the integral in (9) analytic (Blanchard and Sapsis, 2021a,b).

For an illustration of the benefits provided by the likelihood ratio, we consider the (static) Michalewicz function (S12d) with the input space $[0, \pi]^2$ rescaled to the unit square and a Gaussian prior $p_x(\mathbf{z}) = \mathcal{N}(\mathbf{0} + 1/2, 0.01\mathbf{I})$ in space (see Fig. 1). The Michalewicz function is characterized by large regions of “flatland” interrupted by steep valleys and ridges, with its deepest portion accounting for a tiny fraction of the search space. For this function, Fig. 1 makes it visually clear that the likelihood ratio gives more emphasis to the area where the quantity of interest $f(\mathbf{x})$ assumes abnormally small values, taking precedence over the operator’s belief that the UAV should focus solely on the center region. Fig. 1 also shows that $w(\mathbf{x})$ can be approximated satisfactorily with a small number of Gaussian mixtures, a key prerequisite for algorithm efficiency.

4. Results

4.1. Experimental protocol

To solidify the utility of the likelihood ratio in environment exploration, we perform a series of numerical experiments as per the following protocol. For each example considered, the search space is rescaled to the unit square $[0, 1]^2$ and the UAV initial pose is specified as $\mathbf{z}_0 = \mathbf{0}$ and $\theta_0 = \pi/4$. At each iteration, the UAV admissible destinations are constrained to lie on a circular arc with radius L centered at \mathbf{z}_n and subtending an angle 2α which bisects θ . The parameters L and

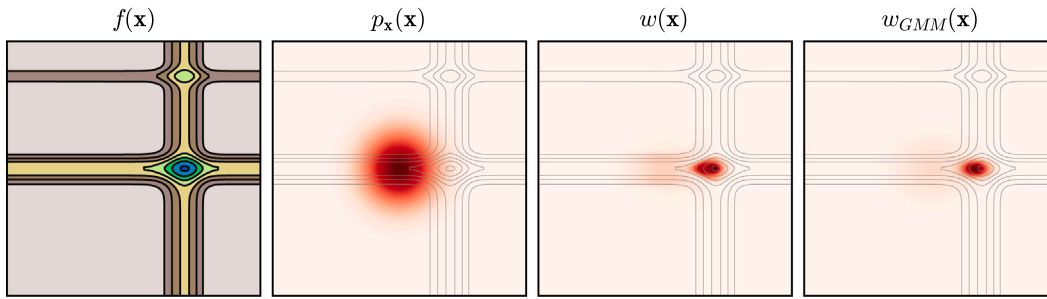


Fig. 1. From left to right: Contour plots of the map $f(\mathbf{x})$, the input prior $p_x(\mathbf{x}) = p_z(\mathbf{z})$, the likelihood ratio $w(\mathbf{x})$, and the GMM approximation of the likelihood ratio $w_{GMM}(\mathbf{x})$ with two Gaussian mixtures.

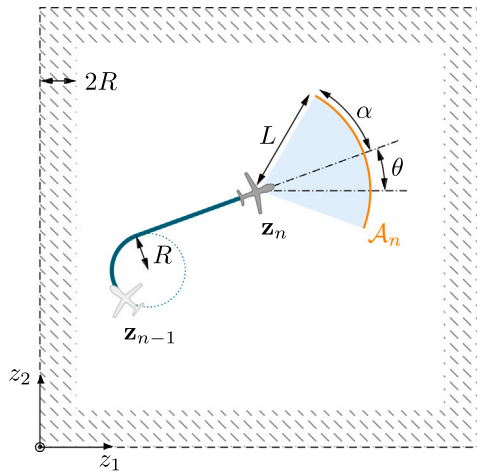


Fig. 2. Schematic of the experimental set-up for environment exploration (not to scale).

α characterize the *lookahead distance* and *field of view* of the UAV, respectively. To avoid situations in which the UAV might venture outside of the search space, we discard from the set of admissible destinations those lying a distance $2R$ or less from the boundaries of the unit square. Each mission takes place over the interval $t \in [0, 15]$, with the UAV traveling at unit speed and collecting measurements every $t_s = 1/15$ time units. A schematic of the experimental set-up is shown in Fig. 2.

To assess performance of the algorithm, we compute the following metrics.

Root mean square error:

$$\text{rmse}(t) = \sqrt{\frac{1}{N} \sum_{i=1}^N [f(\mathbf{z}_i, t) - \mu_t(\mathbf{z}_i, t)]^2}, \quad (13a)$$

where $\{\mathbf{z}_i\}_{i=1}^N$ is a set of 10^5 samples uniformly distributed over the physical domain, and μ_t denotes the posterior mean of the GP model in use by the UAV at time t .

Log-pdf error:

$$\text{pdfe}(t) = \int \left| \log p_{f(\mathbf{z}, t)}(y) - \log p_{\mu_t(\mathbf{z}, t)}(y) \right| dy, \quad (13b)$$

where the densities are estimated using the same 10^5 samples as for the root mean square error.

Distance to minimizer:

$$\ell(t) = \|\mathbf{z}_t^* - \mathbf{z}_t^+\|^2, \quad (13c)$$

where \mathbf{z}_t^* and \mathbf{z}_t^+ are the minimizers for the true map $f(\mathbf{z}, t)$ and the GP mean $\mu_t(\mathbf{z}, t)$, respectively.

Simple regret:

$$r(t) = f(\mathbf{z}_t^+, t) - f(\mathbf{z}_t^*, t). \quad (13d)$$

The root mean square error measures the overall goodness of the GP model with no consideration for anomalies of any kind. In contrast, the log-pdf error judges the model by its ability to reconstruct the tails of the output pdf, which is where abnormal features “live”. The metrics ℓ and r quantify the model ability to predict the locations and output value, respectively, of the map’s global minimizers. These two metrics are appropriate because in the examples considered the global minimizers are associated with abnormally small output values.

On the first iteration, any admissible destination is as good as any other from the UAV’s standpoint because there is only one measurement available (collected at \mathbf{z}_0). To disambiguate the situation, the first destination \mathbf{z}_1 is drawn uniformly from the set of admissible destinations \mathcal{A}_0 . This introduces an element of randomness in the problem, which is averaged out by repeating the mission many times, each time with a different choice of \mathbf{z}_1 . For each example considered, we repeat the mission 50 times, and report the median of the cumulative minimum for the four metrics introduced above. Variability across missions is quantified by the median absolute deviation. Our code is available on GitHub.¹

4.2. Benchmark results for static test functions

We evaluate the performance of the proposed criteria on five static test functions commonly used in optimization and uncertainty quantification: Ackley, Bird, Bukin06, Michalewicz, and Modified Rosenbrock. Analytical expressions are given in Section S2 of the Supplementary Material. These functions were chosen because they are representative of what an anomalous environment may look like in real life. For example, the steep ridge of the Bukin06 function is reminiscent of an unusually deep oceanic trench; and the Ackley function is evocative of a substance diffusing away from an abnormally potent source (Fig. 3).

In each case, the noise variance is specified as $\sigma_n^2 = 10^{-3}$ and appropriately rescaled to account for the variance of the map f . We do not set the parameter σ_n^2 beforehand in the GP model; instead, we let the UAV learn it from data. We use $L = 0.2$, $\alpha = 3\pi/4$, and $R = 0.02$ for the path-planning algorithm, and $n_{GMM} = 2$ for the GMM approximation of the likelihood ratio. In the interest of space, results for the Bird, Bukin06 and Modified Rosenbrock functions have been relegated to the Supplementary Material.

We first consider the situation in which the UAV operator has no prior beliefs about the locations of anomalies in the search space, and thus a uniform prior is used for p_z . For the Ackley and Michalewicz functions, Fig. 4 shows that the proposed LW criteria substantially

¹ <https://github.com/ablancha/gppath>.

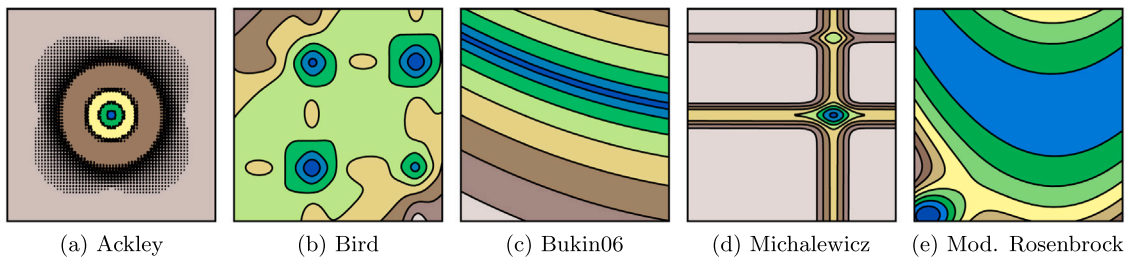


Fig. 3. Contour plots of the test functions considered in Section 4.2.

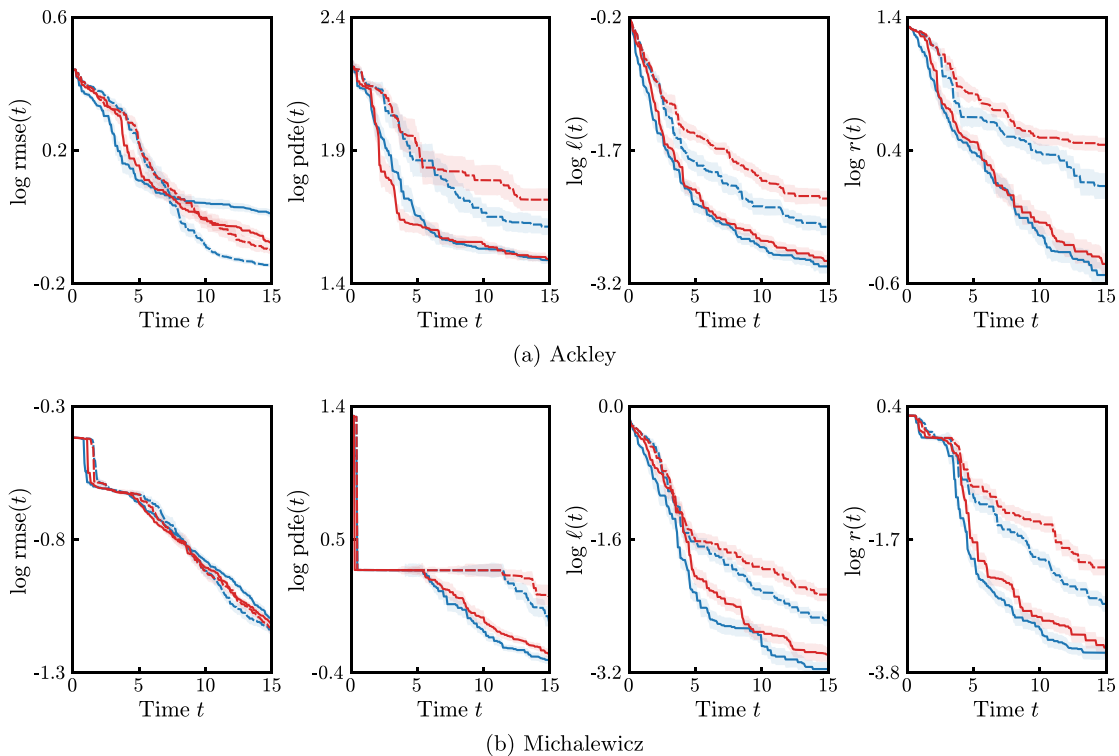


Fig. 4. For uniform p_z , performance of $---$ US; $—$ US-LW; $---$ IVR; $—$ IVR-LW.

outperform their unweighted counterparts in the three critical metrics pdfe, ℓ and r , often by more than one full order of magnitude. This shows that a UAV guided by US-LW or IVR-LW is able to identify environment anomalies more quickly and more efficiently than otherwise (Movies 1a and 1b). When performance is measured in terms of the rmse, US-LW and IVR-LW are on par with US and IVR. This is not surprising since US and IVR are specifically designed for rmse minimization, while US-LW and IVR-LW are not. This is inconsequential from the standpoint of anomaly detection since the rmse only accounts for second-order moments and therefore is not a good indicator of anomalies. Similar trends are seen for the other test functions (Figure S1 and Movies 1c–1e).

We next consider the situation in which the UAV operator has some prior beliefs about where anomalies may be located and therefore decides to specify the same spatial prior as in Fig. 1 to focus exploration in the central part of the domain. For the Ackley function, this is a good guess, and as a result US-IW, US-LW, IVR-IW, and IVR-LW deliver similar performance, as shown in Fig. 5a and Movie 2a. For this function, the likelihood ratio is not particularly helpful. For the other test functions, however, the operator's guess is quite poor, which leads to vastly different outcomes. Fig. 5(b) and S2 as well as Movies 2b–2e are a testament to the likelihood ratio's ability to correct the operator's beliefs and refine the UAV decision making in a way that makes anomaly detection more efficient. Absent the likelihood ratio,

the UAV does not have the ability to override the operator's guidelines, missing out on the critical anomalous features that lie beyond its ascribed area.

In the results presented above, no information was provided to the algorithm regarding the fact that the environment did not depend on time. Consequently, the UAV had to figure this out on its own from the data it had collected. To let the UAV know that the environment is indeed static (as is the case with, for example, topography), the UAV operator may either set the lengthscale associated with the temporal variable in (3) to infinity, or drop the time variable from the GP model altogether. For the Ackley and Michalewicz functions with uniform prior, Figures S3 and S4 show that both approaches produce results that are quantitatively similar to those in Figs. 4 and 5 where time-independence was not explicitly enforced. This demonstrates the ability of the spatiotemporal GP model to infer the critical characteristics of the environment.

4.3. Benchmark results for dynamic test functions

We now investigate the performance of the algorithm under dynamic environmental conditions. We repeat the experiments in Section 4.2 for the dynamic Ackley and Michalewicz functions which are constructed by applying the transformation

$$z_1 \rightarrow z_1 + 0.1 \sin(2\pi t/15) \pmod{1}$$

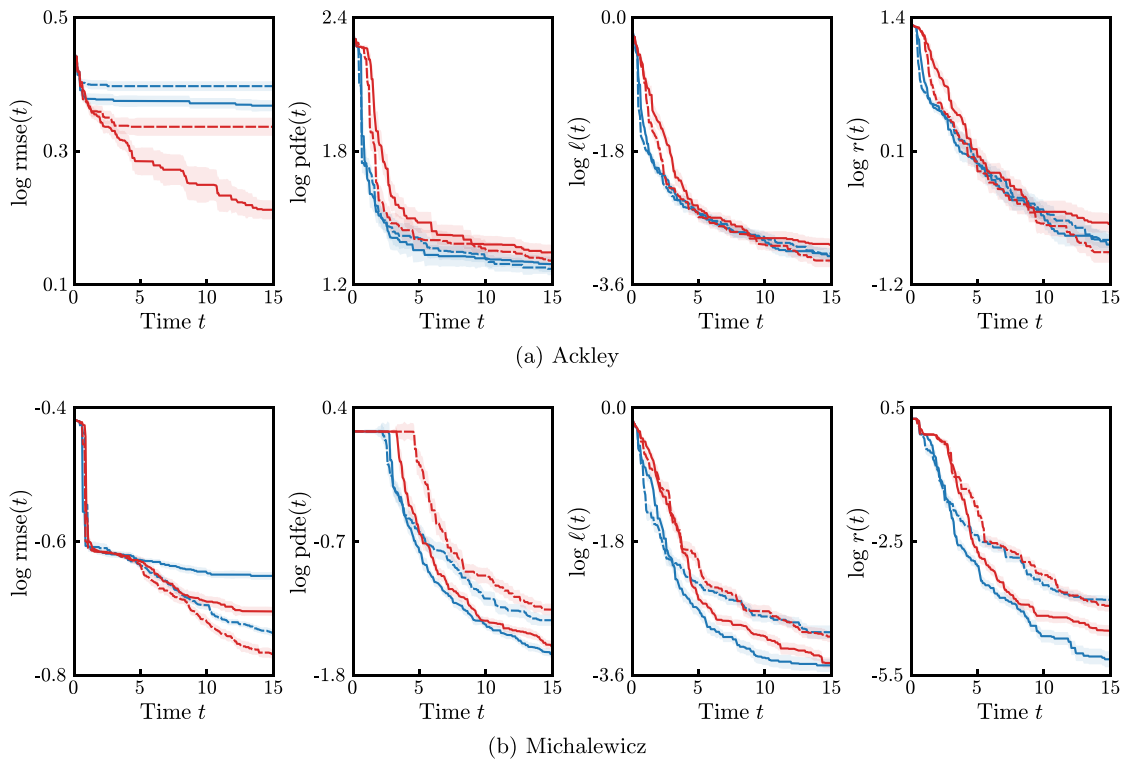


Fig. 5. For Gaussian p_z , performance of — US-IW; — US-LW; - - IVR-IW; — IVR-LW.

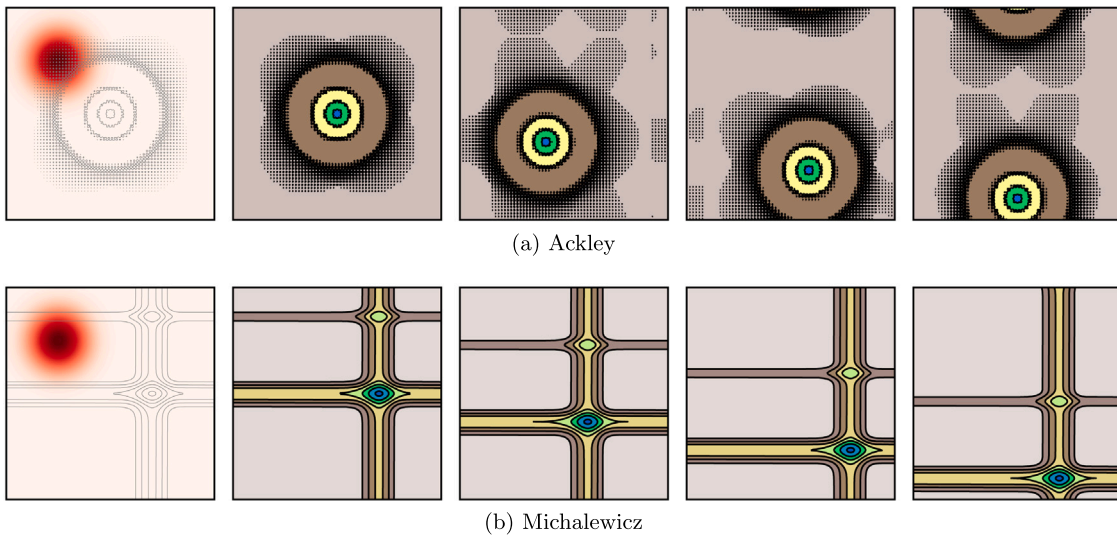


Fig. 6. From left to right: Contour plots of the adversarial input prior p_z (leftmost panel) and the map $f(z, t)$ at $t = 0, 5, 10$ and 15 (four rightmost panels).

$$z_2 \rightarrow 0.4t/15 \pmod 1$$

to the physical space $[0, 1]^2$. (The modulo operator ensures periodicity of the resulting functions across the domain boundaries.) We use a strongly adversarial Gaussian prior, $p_z = \mathcal{N}([0.25, 0.75]^T, 0.01\mathbf{I})$, whose mass is primarily distributed in the upper left corner of the domain, quite far from any noteworthy environmental feature (see Fig. 6).

For the same parameters as in Section 4.2 ($\sigma_n^2 = 10^{-3}$, $L = 0.2$, $\alpha = 3\pi/4$, $R = 0.02$, and $n_{GMM} = 2$), Fig. 7 show that the presence of the likelihood ratio significantly improves algorithm performance despite the added difficulty arising from the environment being dynamic and the input prior being severely misleading (see also Movies 3a and 3b). These results illustrate the utility of the likelihood ratio for dynamic tracking of anomalies in strongly adversarial conditions. We note,

however, that the tracking of extremes cannot be perfect since the drone operates with limited resources and therefore must find a delicate balance between exploring the space, keeping track of the anomalies, and trusting or overcoming the prior.

4.4. Application to real-world bathymetry data

Bathymetric anomalies are important for the telecommunications industry and the oil and gas industry to be able to build subsea infrastructure, and also for navigation and coastal management as well as tsunami forecasting (Tani, 2017). Here we consider the problem of reconstructing the topography of the seafloor near the Izu–Ogasawara trench, an oceanic trench located in the western Pacific Ocean and

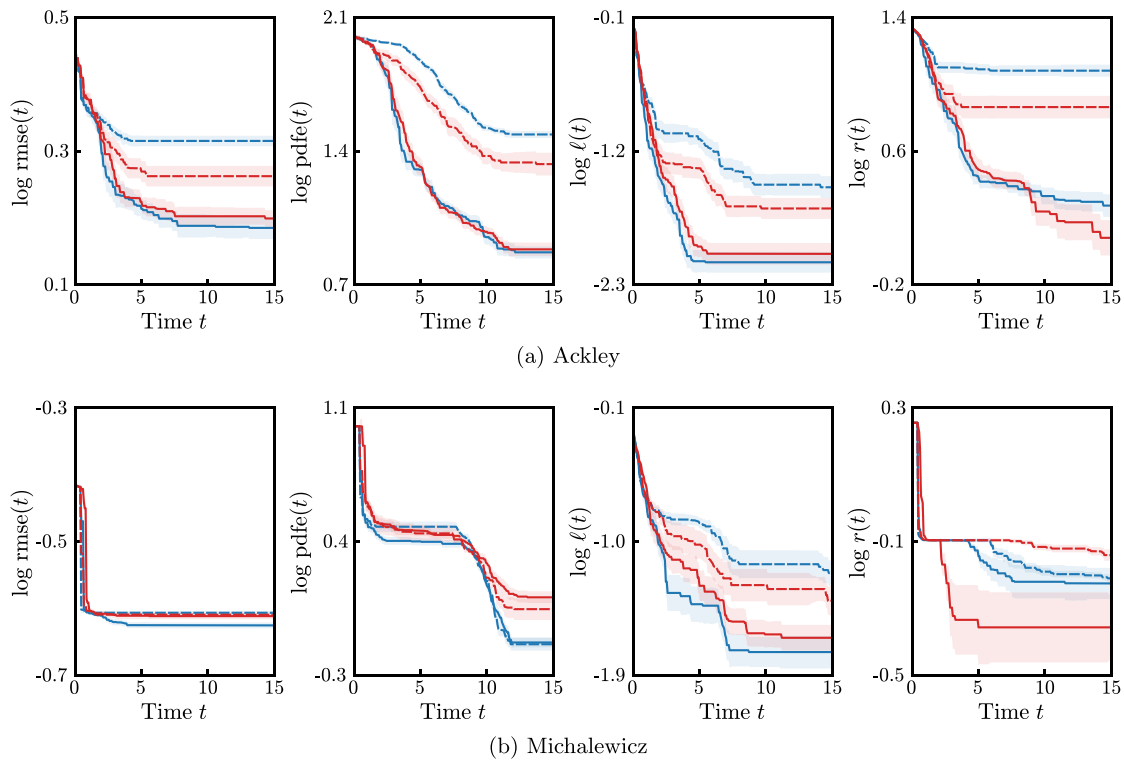


Fig. 7. For the dynamic test functions with strongly adversarial prior shown in Fig. 6, performance of — US-IW; — US-LW; - - IVR-IW; — IVR-LW.

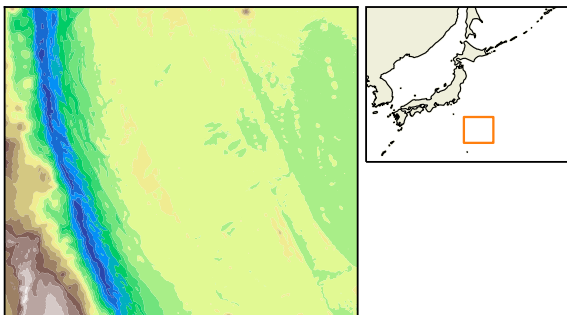


Fig. 8. Contour plot of the Izu-Ogasawara bathymetric profile located off the coast of Japan.

stretching from Japan to the northernmost section of the Mariana Trench. The UAV is directed to explore an area of about 92,000 square miles (about 240,000 square kilometers) which is mostly flat, except for the trench itself whose deepest point is at about 32,000 ft (about 9800 m) below sea level. The trench, therefore, constitutes a strong anomaly relative to the rest of the environment (Fig. 8).

The true map f is constructed by fitting a cubic spline to gridded bathymetric data made available by GEBCO.² Since the dataset consists of real-world measurements, there is no need to corrupt it with artificial noise; we just let the UAV learn the value of the noise variance σ_n^2 from the raw data recorded during the mission. Because the search space is rescaled to the unit square (see Section 4.1), we use the same parameters for the path-planning algorithm as in the previous sections ($L = 0.2$, $\alpha = 3\pi/4$, and $R = 0.02$). For the GMM approximation of the likelihood ratio, we use $n_{GMM} = 2$.

Fig. 9a shows that when no hint is given to the UAV prior to the mission (i.e., uniform p_z), the likelihood-weighted acquisition functions lead to marginally better performance compared to the unweighted criteria. On the other hand, Fig. 9b shows that when the UAV is given inaccurate prior information about the location of the trench (i.e., same Gaussian p_z as in Fig. 1), the likelihood-weighted acquisition functions perform substantially better than the unweighted criteria. These results illustrate the power of the likelihood ratio to overcome adversarial beliefs, which is particularly valuable in situations where a malicious agent attempts to seize control of the UAV and lead it astray.

5. Conclusions

We have introduced two novel acquisitions functions for informative path planning that are specifically designed for identification of anomalies in exploration missions. Having ramifications running deep within the field of rare-event quantification, the proposed criteria exploit the unique properties of the likelihood ratio to guide the UAV toward areas in which the quantity of interest is thought to exhibit strong anomalies. We applied the proposed algorithm to a number of synthetic test functions as well as a real-world bathymetry dataset. Overall, the likelihood-weighted criteria led to faster identification of anomalies present in the environment, especially in adversarial settings.

Our approach can be adapted for use with more sophisticated path-planning algorithms and in more complex environments. The two-dimensional Dubins path parametrization used in this work can be extended to a three-dimensional search space using the implementation of Owen et al. (2014). As discussed in Section 2.2, more complex time-dependence of the environment can be accommodated by using a covariance function that encodes specific spatiotemporal relationships (Singh et al., 2010; Krause and Ong, 2011; Marchant and Ramos, 2014). This is important from the standpoint of environment surveillance. Localization noise can also be accounted for using the algorithm of Oliveira et al. (2019, 2020).

Our method is quite general and therefore has positive implications for a range of commercial, scientific, and military applications in which

² <https://www.gebco.net>.

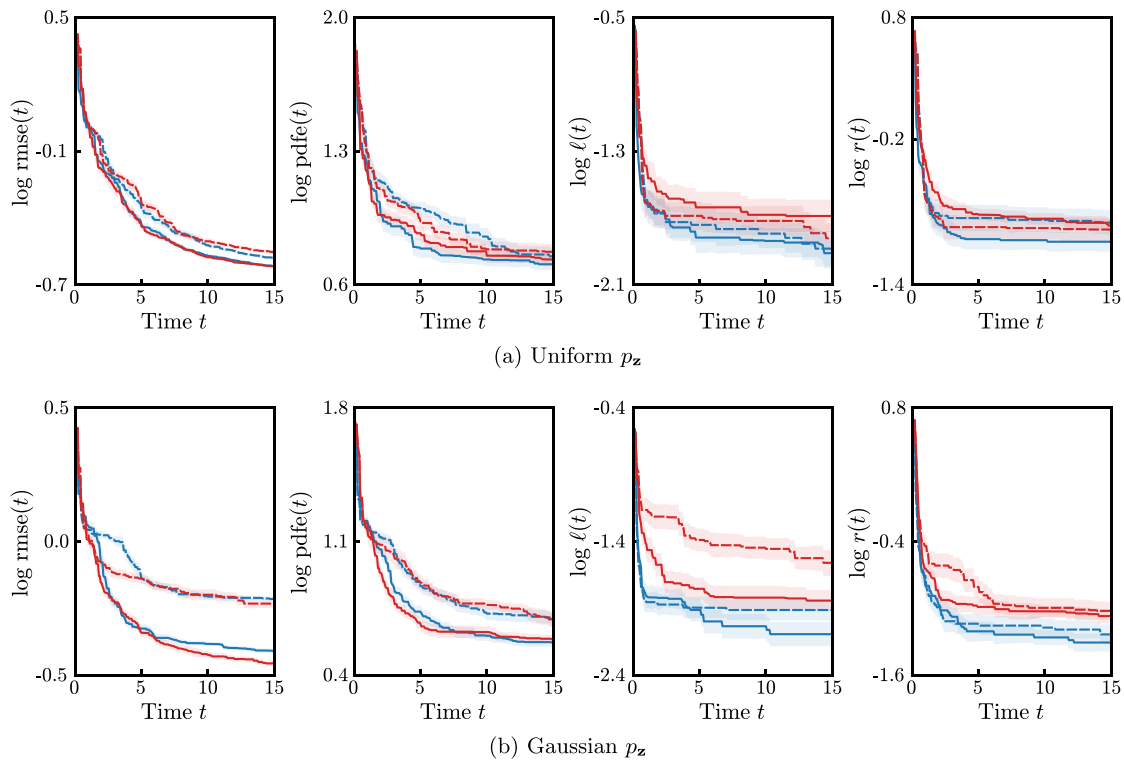


Fig. 9. For the Izu-Ogasawara bathymetric profile, performance of — US(-IW); — US-LW; - - IVR(-IW); — IVR-LW.

anomaly detection is critical. For underwater UAVs, our approach can be used to make detailed maps of the seafloor, of which less is known than of the topography of Mars (Tani, 2017). In the Arctic region, bathymetry can be used to map the fjords' sill depths, a key indicator for the rise in global sea level. Our method can also improve detection of wreckages of missing crafts as well as other artifacts found in underwater archeological sites, which may be viewed as abnormal features lying on the ocean floor.

For aerial UAVs, our work can be used to detect abnormal concentrations of chemicals, pollutants, or radioactive material in a region of interest; to reconstruct terrain with unknown topography in order to plan large-scale architecture; and to monitor abnormal crop growth in order to optimize agriculture operations. In the military, our algorithm can facilitate the clearing of minefields, having the ability to quickly identify signs of explosive chemicals leaking from landmines and causing abnormalities in the surrounding vegetation (University of Bristol, 2016).

CRediT authorship contribution statement

Antoine Blanchard: Conceptualization, Investigation, Methodology, Software, Validation, Visualization, Writing. **Themistoklis Sapsis:** Conceptualization, Funding acquisition, Investigation, Methodology, Project administration, Resources, Supervision, Validation, Writing – review & editing.

Declaration of competing interest

The authors declare that they have no known competing financial interests or personal relationships that could have appeared to influence the work reported in this paper.

Acknowledgments

The authors acknowledge support from the Air Force Office of Scientific Research (MURI Grant No. FA9550-21-1-0058), the Army Research Office (Grant No. W911NF-17-1-0306) and the 2020 MathWorks Faculty Research Innovation Fellowship.

Appendix A. Supplementary data

Supplementary material related to this article can be found online at <https://doi.org/10.1016/j.oceaneng.2021.110242>.

References

- Albeverio, S., Jentsch, V., Kantz, H., 2006. *Extreme Events in Nature and Society*. Springer, New York.
- Bai, S., Wang, J., Chen, F., Englot, B., 2016. Information-theoretic exploration with Bayesian optimization. In: *IEEE/RSJ International Conference on Intelligent Robots and Systems*. pp. 1816–1822.
- Beck, J., Guillas, S., 2016. Sequential design with mutual information for computer experiments (MICE): Emulation of a tsunami model. *SIAM J. Uncertain. Quantif.* 4, 739–766.
- Blanchard, A., Sapsis, T., 2021a. Bayesian optimization with output-weighted optimal sampling. *J. Comput. Phys.* 425, 109901.
- Blanchard, A., Sapsis, T., 2021b. Output-weighted importance sampling for Bayesian experimental design and uncertainty quantification. *SIAM J. Uncertain. Quantif.* 9, 564–592.
- Brochu, E., Cora, V.M., De Freitas, N., 2010. A tutorial on Bayesian optimization of expensive cost functions, with application to active user modeling and hierarchical reinforcement learning. *arXiv preprint arXiv:1012.2599*.
- Chaloner, K., Verdinelli, I., 1995. Bayesian experimental design: A review. *Statist. Sci.* 10, 273–304.
- Cohn, D.A., 1994. Neural network exploration using optimal experiment design. In: *Advances in Neural Information Processing Systems*. pp. 679–686.
- Dubins, L.E., 1957. On curves of minimal length with a constraint on average curvature, and with prescribed initial and terminal positions and tangents. *Amer. J. Math.* 79, 497–516.
- Dunbabin, M., Marques, L., 2012. Robots for environmental monitoring: Significant advancements and applications. *IEEE Robot. Autom. Mag.* 19, 24–39.
- Embrechts, P., Klüppelberg, C., Mikosch, T., 2013. *Modeling Extremal Events for Insurance and Finance*. Springer, New York.
- Flaspohler, G., Roy, N., Girdhar, Y., 2018. Near-optimal irrevocable sample selection for periodic data streams with applications to marine robotics. In: *International Conference on Robotics and Automation*. pp. 1–8.
- Gramacy, R.B., Lee, H.K.H., 2009. Adaptive design and analysis of supercomputer experiments. *Technometrics* 51, 130–145.
- Guestrin, C., Krause, A., Singh, A.P., 2005. Near-optimal sensor placements in Gaussian processes. In: *Proceedings of the 22nd International Conference on Machine Learning*. pp. 265–272.

- Higdon, D., 2002. Space and space-time modeling using process convolutions. In: *Quantitative Methods for Current Environmental Issues*. Springer, pp. 37–56.
- Hitz, G., Galceran, E., Garneau, M.-E., Pomerleau, F., Siegwart, R., 2017. Adaptive continuous-space informative path planning for online environmental monitoring. *J. Field Robotics* 34, 1427–1449.
- Huang, S., Teo, R.S.H., 2019. Computationally efficient visibility graph-based generation of 3D shortest collision-free path among polyhedral obstacles for unmanned aerial vehicles. In: 2019 International Conference on Unmanned Aircraft Systems (ICUAS). IEEE, pp. 1218–1223.
- Jones, D.R., Schonlau, M., Welch, W.J., 1998. Efficient global optimization of expensive black-box functions. *J. Global Optim.* 13, 455–492.
- Kleijnen, J.P.C., Van Beers, W.C.M., 2004. Application-driven sequential designs for simulation experiments: Kriging metamodeling. *J. Oper. Res. Soc.* 55, 876–883.
- Krause, A., Ong, C.S., 2011. Contextual Gaussian process bandit optimization. In: *Advances in Neural Information Processing Systems*. pp. 2447–2455.
- Lam, C.Q., 2008. *Sequential Adaptive Designs in Computer Experiments for Response Surface Model Fit* (Ph.D. thesis). The Ohio State University.
- MacKay, D.J.C., 1992. Information-based objective functions for active data selection. *Neural Comput.* 4, 590–604.
- Marchant, R., Ramos, F., 2012. Bayesian optimisation for intelligent environmental monitoring. In: *IEEE/RSJ International Conference on Intelligent Robots and Systems*. pp. 2242–2249.
- Marchant, R., Ramos, F., 2014. Bayesian optimisation for informative continuous path planning. In: *IEEE International Conference on Robotics and Automation*. pp. 6136–6143.
- Martinez-Cantin, R., De Freitas, N., Brochu, E., Castellanos, J., Doucet, A., 2009. A Bayesian exploration-exploitation approach for optimal online sensing and planning with a visually guided mobile robot. *Auton. Robots* 27, 93–103.
- Meliou, A., Krause, A., Guestrin, C., Hellerstein, J.M., 2007. Nonmyopic informative path planning in spatio-temporal models. In: *AAAI*, Vol. 10. pp. 16–17.
- Mohamad, M.A., Sapsis, T.P., 2018. Sequential sampling strategy for extreme event statistics in nonlinear dynamical systems. *Proc. Natl. Acad. Sci.* 115, 11138–11143.
- Morere, P., Marchant, R., Ramos, F., 2016. Bayesian optimisation for solving continuous state-action-observation POMDPs. In: *Advances in Neural Information Processing Systems*. pp. 1–5.
- Morere, P., Marchant, R., Ramos, F., 2017. Sequential Bayesian optimization as a POMDP for environment monitoring with UAVs. In: *IEEE International Conference on Robotics and Automation*. pp. 6381–6388.
- Oliveira, R., Ott, L., Guizilini, V., Ramos, F., 2020. Bayesian optimisation for safe navigation under localisation uncertainty. In: *Robotics Research*. Springer, Cham, Switzerland, pp. 489–504.
- Oliveira, R., Ott, L., Ramos, F., 2019. Bayesian optimisation under uncertain inputs. *arXiv preprint arXiv:1902.07908*.
- Owen, A.B., 2013. *Monte Carlo Theory, Methods and Examples*. Published online at <https://statweb.stanford.edu/~owen/mc>.
- Owen, M., Beard, R.W., McLain, T., 2014. Implementing dubins airplane paths on fixed-wing UAVs. In: Valavanis, K.P., Vachtsevano, G.J. (Eds.), *Handbook of Unmanned Aerial Vehicles*. Springer, Dordrecht, pp. 1677–1701, chap. 68.
- Rasmussen, C.E., Williams, C.K.I., 2006. *Gaussian Processes for Machine Learning*. MIT Press, Cambridge, MA.
- Reggente, M., Lilienthal, A.J., 2009. Using local wind information for gas distribution mapping in outdoor environments with a mobile robot. In: *SENSORS, 2009 IEEE*. IEEE, pp. 1715–1720.
- Sacks, J., Welch, W.J., Mitchell, T.J., Wynn, H.P., 1989. Design and analysis of computer experiments. *Statist. Sci.* 4, 409–423.
- Sapsis, T.P., 2020. Output-weighted optimal sampling for Bayesian regression and rare event statistics using few samples. *Proc. R. Soc. Lond. Ser. A Math. Phys. Eng. Sci.* 476, 20190834.
- Shahriari, B., Swersky, K., Wang, Z., Adams, R.P., De Freitas, N., 2015. Taking the human out of the loop: A review of Bayesian optimization. *Proc. IEEE* 104, 148–175.
- Singh, A., Krause, A., Kaiser, W.J., 2009. Nonmyopic adaptive informative path planning for multiple robots. In: *Twenty-First International Joint Conference on Artificial Intelligence*. pp. 1–11.
- Singh, A., Ramos, F., Whyte, H.D., Kaiser, W.J., 2010. Modeling and decision making in spatio-temporal processes for environmental surveillance. In: *IEEE International Conference on Robotics and Automation*. pp. 5490–5497.
- Srinivas, N., Krause, A., Kakade, S.M., Seeger, M., 2009. Gaussian process optimization in the bandit setting: No regret and experimental design. *arXiv preprint arXiv:0912.3995*.
- Stachniss, C., Grisetti, G., Burgard, W., 2005. Information gain-based exploration using Rao-Blackwellized particle filters. In: *Robotics: Science and Systems*, Vol. 2. pp. 65–72.
- Tani, S., 2017. *Understanding Oceans*, Vol. 1. The UNESCO Courier, pp. 65–69.
- University of Bristol, 2016. *Bristol Scientists Fly Drone over Old Trafford to Research Landmine Clearance*. Press release, <http://www.bristol.ac.uk/news/2016/april/drone-over-old-trafford.html>.
- Verdinelli, I., Kadane, J.B., 1992. Bayesian designs for maximizing information and outcome. *J. Amer. Statist. Assoc.* 87, 510–515.
- Zhang, X., Huang, S., Liang, W., Cheng, Z., Tan, K.K., Lee, T.H., 2019. HLT*: Real-time and any-angle path planning in 3D environment. In: *IECON 2019-45th Annual Conference of the IEEE Industrial Electronics Society*, Vol. 1. IEEE, pp. 5231–5236.